

Electrochemical Investigation of Pt-Co/MWCNT as an Alcohol-Tolerant ORR Catalyst for Direct Oxidation Fuel Cells

D. Morales-Acosta¹, D. López de la Fuente², L.G. Arriaga¹, G. Vargas Gutiérrez² and F. J. Rodríguez Varela^{2,}*

¹ Centro de Investigación y Desarrollo Tecnológico en Electroquímica, Parque Tecnológico Querétaro, Sanfandila, Pedro Escobedo, C. P. 76703 Querétaro, México

² Cinvestav Unidad Saltillo, Carr. Saltillo-Monterrey Km. 13.5, Ramos Arizpe, Coahuila, C.P. 25900, México.

*E-mail: javier.varela@cinvestav.edu.mx

Received: 15 March 2011 / *Accepted:* 11 May 2011 / *Published:* 1 June 2011

In this study, we investigated the behavior of a 30% Pt₇₀-Co₃₀/MWCNT electrocatalyst as oxygen reduction reaction (ORR) material in acid electrolyte without and with liquid fuels. The characterization was performed by rotating ring-disc electrode (RRDE) and electrochemical impedance spectroscopy (EIS). In the absence of organic molecules, the ORR on the alloy proceeds via a 4-electron transfer mechanism, with a negligible production of hydrogen peroxide, as indicated by the RRDE measurements. In the presence of the different liquid fuels (ethylene glycol, ethanol or 2-propanol), the alloy shows a high degree of tolerance, although this characteristic is dependent on the chemical composition of the molecule. The EIS measurements in solutions containing organic molecules suggest that at high polarization potentials, the competitive interaction of oxygen reduction and liquid fuels oxidation at the alloy catalytic sites leads to a faster reaction, as shown by the smaller charge transfer resistances (R_{ct}) obtained from Nyquist plots, compared to the R_{ct} values without organic molecules. The results obtained from the Pt-Co/MWCNT electrocatalyst are compared to those of a commercial Pt/C cathode.

Keywords: Tolerant cathodes, oxygen reduction reaction, Pt-alloys, EIS, direct oxidation fuel cells

1. INTRODUCTION

The results obtained recently by different research groups worldwide, clearly indicate that the crossover of liquid fuels through commercially available polymer electrolyte membranes is a very important drawback for the commercialization of low temperature Direct Oxidation Fuel Cells (DOFCs) [1-5]. When Pt-alone electrocatalysts are used as cathodes in this type of cells, large

efficiency losses appear because Pt is rapidly poisoned by such substances and/or their intermediates [1, 2].

Under these circumstances, studies covering highly active and selective cathodes have been very dynamic in the past decade. The investigations on this matter include tolerant cathodes based on Pt alloys (Pt-M/C, where M= Cr, Co, Fe, Ni, among others) which have shown a high catalytic activity for the ORR [1, 3, 6-8]. In some cases, their performance for the ORR has surpassed that of Pt/C cathodes [1, 8].

The enhanced catalytic activity of Pt-M/C electrocatalysts for the ORR has been attributed to changes in the electronic structure [9] or to favorable variations in the Pt-Pt interatomic distances [10] due to the alloy formation.

Furthermore, it was recently suggested that a more complex scenario that involves several experimental parameters and choice of materials may positively influence the catalytic activity of Pt-alloys for the ORR [7]. At the same time, investigations of the selectivity of Pt-alloys have clearly pointed out to their high degree of tolerance to the presence of organic substances [1, 3, 7]. As a result, the polarization studies in O₂-saturated solutions containing liquid fuels have shown negligible shifts in ORR overpotentials at Pt-based alloys.

In addition, no current density peaks due to the oxidation of the organic molecules emerged at these cathodes during potential polarizations, making such materials remarkable candidates for DOFCs applications [1, 3, 7, 11].

Meanwhile, a variety of fuels have been tested in DOFCs. The direct oxidation of ethanol (EtOH, C₂H₅OH) [3, 12, 13], ethylene glycol (EG, C₂H₆O₂) [14, 15, 16] or 2-propanol (2-Prop, C₃H₈O) [4, 5, 17] has been studied as an alternative to the use of methanol (MeOH, CH₃OH). The results reported in those references indicate that the alternative fuels could be oxidized at low temperatures on suitable electrocatalysts to produce CO₂, along with some intermediates. Furthermore, the toxicity and ecotoxicity of C₂H₅OH, C₂H₆O₂ and C₃H₈O has been reported to be lower than that of CH₃OH [18].

These characteristics make these fuels of considerable interest for DOFCs applications. This issue is very important because high performance DOFCs operating with liquid fuels having low toxicity must be developed in order to advance in the commercialization of these devices. However, we should keep in mind that under operating conditions, the 3 alternative fuels mentioned here-above may permeate through commercially available membranes [3, 4, 19]. Therefore, in a simultaneous effort, cathode electrocatalysts with high tolerance to C₂H₅OH, C₂H₆O₂ and C₃H₈O should also be developed.

In this work, we report the synthesis, characterization and performance of a Pt₇₀-Co₃₀/MWCNT electrocatalyst for the ORR under DOFCs conditions. MWCNTs were the support of choice because of their reported advantages over Vulcan, regarding the higher durability and stability observed at nanotubes [20]. The electrochemical behavior of the alloy was studied by RRDE and EIS techniques. The results were compared to those measured for a commercial 20% Pt/C catalyst (E-Tek) under the same conditions.

2. EXPERIMENTAL

2.1. Reagents

Ultrapure 18.3 M Ω deionized water (DI), high-purity N₂ and O₂, as well as analytical grade H₂SO₄, C₂H₅OH, C₂H₆O₂ and C₃H₈O (Aldrich) solutions were used during the experiments.

2.2. Physicochemical characterization

X-ray diffractograms (XRD) of Pt-Co/MWCNT and Pt/C were acquired over 20-100 degrees with 0.05 steps in an X-Pert MPD Phillips apparatus equipped with a curved graphite monochromator using CuK α radiation, operating at 43 kV and 30 mA. A JEOL JSM 5800-LV scanning electron microscope (SEM) was used for energy dispersive X-ray analyses (EDS). HRTEM studies of Pt-Co/MWCNT were carried out in a field emission gun microscope FEI-TITAN 80-300 kV, operated at 300 kV.

2.3. Synthesis procedure for the MWCNTs and supported Pt-Co

The MWCNTs were synthesized by the spray pyrolysis technique. The detailed procedure was already reported in reference [6]. Prior to their use as support and in order to promote their functionalization, the MWCNTs were introduced in a HNO₃/H₂SO₄ (1:4 V/V) solution at 60° C for 5 h under refluxing and stirring conditions. Then, the wet powders were washed with deionized water until the pH of the filtrated solution was 7. Finally, the obtained powders were dried over night at 60° C.

The 30% Pt-Co (70:30 a/o)/MWCNT electrocatalyst was prepared by the impregnation method, with NaBH₄ as reducing agent. MWCNTs were first dispersed in 100 ml deionized water and treated in an ultrasonic bath for 60 minutes. (NH₄)₂PtCl₆ (Stream Chemicals, 99%) and CoN₂O₆·6H₂O (Acros Organic, 99%) in aqueous solution were added into the solution containing MWCNTs. NaBH₄ (Sigma Aldrich, 98.5%) was slowly dropped into this mixture and vigorously stirred for 1 h. The resulting solution was filtered, washed and dried over night at 60° C.

2.4. Electrode preparation and electrochemical set-up

The experimental details regarding the preparation of the catalytic inks have been described elsewhere [2, 21]. A brief description is as follows: separate mixtures containing each of the electrocatalysts, DI water and Nafion (5% wt, DuPont) were prepared by ultrasound to form an ink of 5 mg_{catal}/mL. Then, an aliquot of 10 μ L of Pt-Co or Pt was dispersed onto a glassy carbon disc (mirror polished with 0.05 μ m alumina) fixed in an electrode support.

After drying overnight, the disc covered by the thin film electrocatalyst was used as the working electrode. In a typical experiment, the electrocatalysts were first activated by cyclic voltammetry in N₂ saturated electrolyte (0.5M H₂SO₄) for at least 30 minutes, until reproducible voltammograms were obtained (not shown). Then, the electrolyte was purged with O₂ for at least 15

min., before linear scan voltammograms (LSV) of the ORR were performed in the potential range of 1 to 0.05 V vs. RHE in a RRDE/bipotentiostat fixture (AFCEBP1, Pine Inst.) under rotating conditions (400, 800, 1200 and 1600 rpm). All experiments were performed at the scan rate of 10 mV/s at 25°C. A platinum mesh and an Ag/AgCl were used as counter and reference electrodes, respectively. In order to sense the H₂O₂ formation, the ring potential was kept at 1.2 V vs. RHE. Current or current density values (considering the geometric area of the 5 mm diam. glassy carbon support) were used depending on the plot. For tolerance tests, LSVs in the presence of C₂H₅OH, C₂H₆O₂ or C₃H₈O (0.5M in all cases) were carried out at 1600 rpm, in the same potential range mentioned above.

EIS measurements were acquired with a Voltalab PZ301 potentiostat. The frequency range was 100 kHz to 50 mHz (at 10 points/decade) with an AC perturbation signal of 10 mV. Prior to the acquisition of impedance data, a potential E (the same potential at which impedance measurements were taken afterwards) was applied during 90 s with the working electrode rotating at 1600 rpm. Under these conditions, steady-state was achieved (i.e., when the current response did not vary with time). After this elapsed time, EIS spectra were acquired at the same E value, i.e., 854, 754, 654, 504, 404 and 304 mV vs. RHE in the O₂-saturated electrolyte without and with organic molecules, maintaining $\omega=1600$ rpm. The experimental EIS results were fitted with the aid of the LEVM software in order to obtain the charge transfer resistance (R_{ct}) values.

3. RESULTS AND DISCUSSION

3.1. Physicochemical characterization

Figure 1 shows the XRD patterns of the home-prepared Pt-Co/MWCNT alloy and the commercial Pt/C catalysts. The diffractogram of Pt-Co/MWCNT indicates the formation of a single phase material with a face-centered cubic (fcc) structure. The diffraction peak at 26 (2-theta) degrees is due to the (0 0 2) reflection of hexagonal carbon. The diffraction peaks at about 40, 46, 68, 81 and 86 (2-theta) degrees are due to the Pt (1 1 1), (2 0 0), (2 2 0), (3 1 1), and (2 2 2) reflections, respectively, which represent the typical characteristics of the Pt phase. From the diffractogram, it is evident that the addition of Co forms an alloy structure, confirmed by the shift in the reflection peaks toward higher 2-theta values related to Pt/C. As a consequence, the lattice parameter of Pt-Co/MWCNT is reduced by contraction to 3.885 Å, compared to the lattice parameter of Pt/C estimated to be 3.917 Å.

The average particle sizes for Pt-Co/MWCNT and Pt/C can be obtained from the (2 2 0) reflections with the aid of the Scherrer equation [2]

$$d = \frac{0.9\lambda_{K\alpha 1}}{\beta_{(2\theta)} \cos(\theta)_{\max}} \quad (1)$$

where d is the average particle size, λ is the X-ray wavelength for Cu K α radiation (1.5406 Å), $\beta_{2\theta}$ is the width at half height of the diffraction peak and θ is the angle corresponding to the peak

maximum. The mean particle size of Pt-Co/MWCNT is slightly larger than that of Pt/C, i.e., 6.3 and 2.2 nm, respectively. The physicochemical characteristics of both catalysts are shown in Table 1.

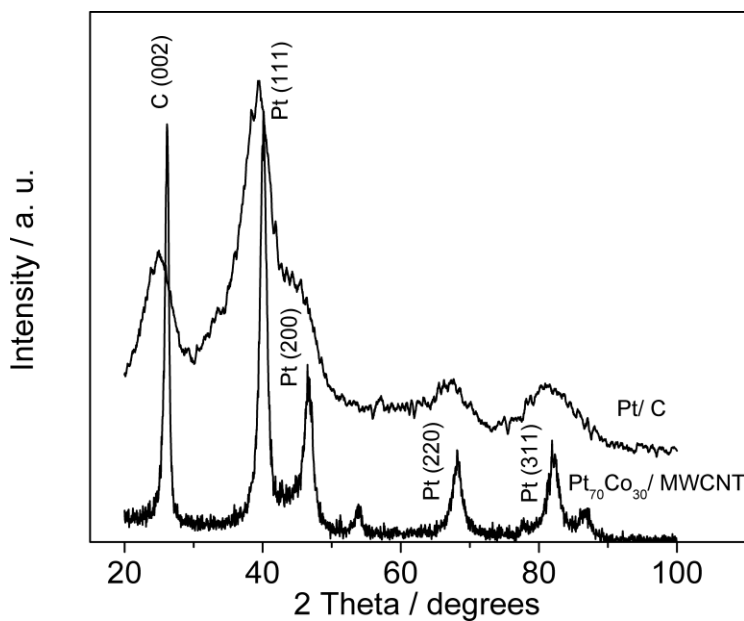


Figure 1. XRD patterns of Pt-Co/MWCNT and Pt/C.

Table 1. Chemical composition and physicochemical characteristics of Pt-Co and Pt.

Catalyst	Lattice parameter (Å)	EDX (at. %)	d (nm) XRD	d (nm) TEM
Pt-Co	3.885	Pt ₇₅ -Co ₂₅	6.3	8
Pt	3.917	-	2.2	2.1

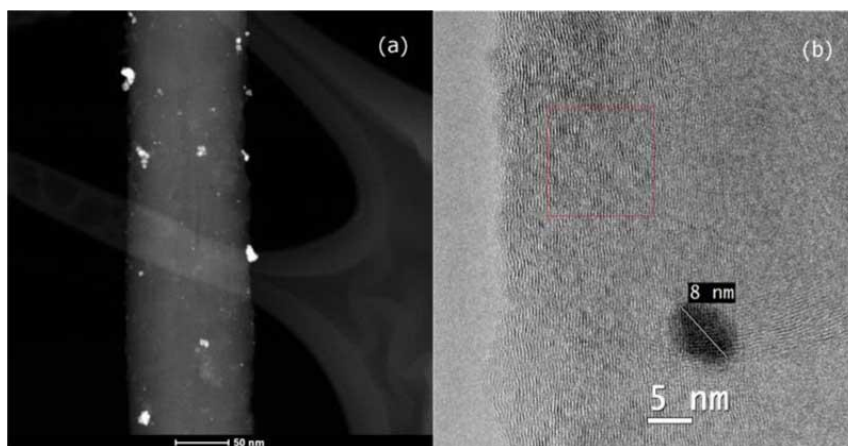


Figure 2. HRTEM images of Pt-Co/MWCNT.

Figure 2 shows high resolution STEM and TEM images of the Pt-Co/MWCNT electrocatalyst. The dispersion along the nanotube is not as highly homogeneous (Figure 2a) as the dispersion of Pt/C (images not shown). The formation of some Pt-Co agglomerates is evident from the image. Figure 2(b) shows the detail of a Pt-Co nanoparticle of around 8 nm size, which is the average particle size determined from TEM after analyzing different areas of this material. These results are consistent with the values obtained from XRD (see average particle sizes values in Table 1).

3.2. ORR mechanism at Pt-Co/MWCNT

Figures 3 and 4 show the disc (i_d) and ring (i_r) currents under rotating conditions at Pt/C and Pt-Co/MWCNT, respectively. The characteristic of kinetic, mixed and diffusion limited regions of i_d are clearly observed in both cases. Overall, the commercial Pt/C shows a higher activity for the ORR than Pt-Co/MWCNT, i.e., lower overpotentials and higher ORR currents in the potential range scanned.

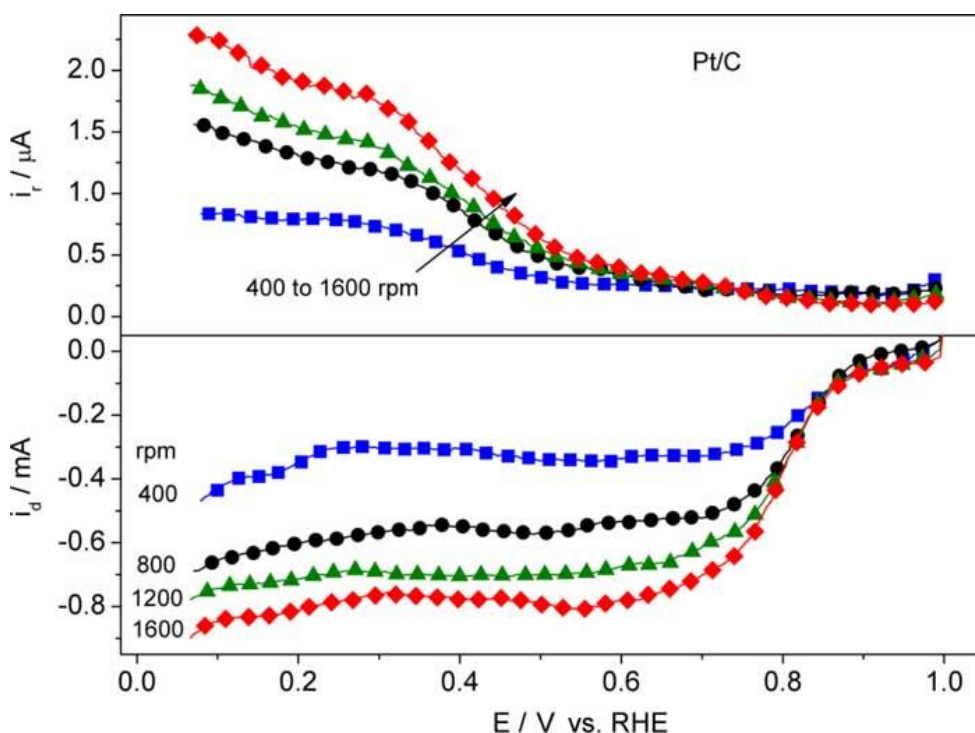


Figure 3. RRDE results at Pt/C in 0.5M H₂SO₄. Scan rate: 10 mV/s. Ring potential held at 1.2 V vs RHE.

With the Levich equation (2), a relationship between the disc current density (j_d) and the kinetic current density (j_k) can be established. Nafion layer diffusion parameters have no effect in the shape of the curves in Figures 3 and 4 because the amount of Nafion used in this study is very small [22]:

$$\frac{1}{j} = \frac{1}{j_k} + \frac{1}{j_d} = \frac{1}{j_k} + \frac{1}{B\omega^{1/2}} \quad (2)$$

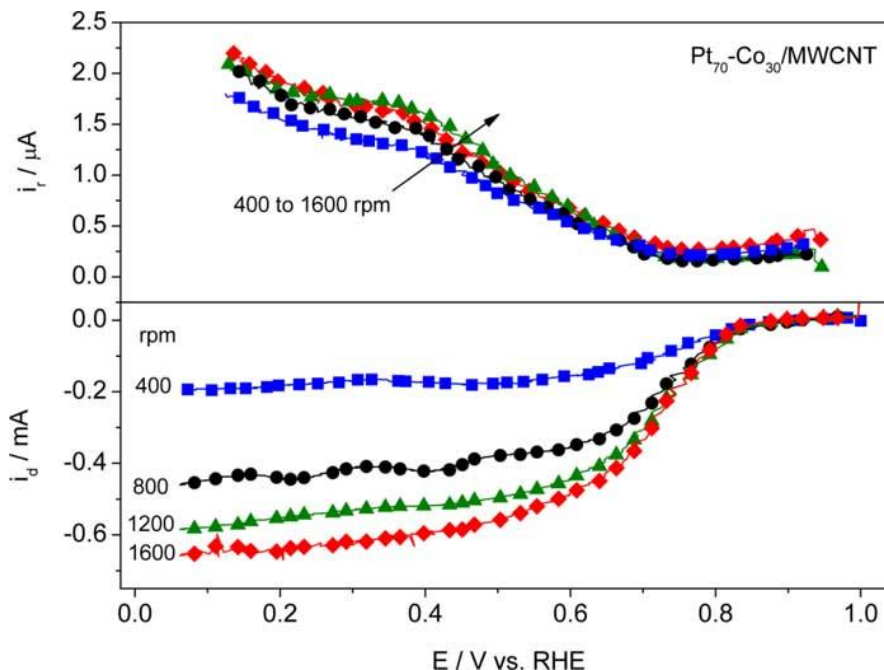


Figure 4. RRDE results at Pt-Co/MWCNT. Same conditions as in Figure 2.

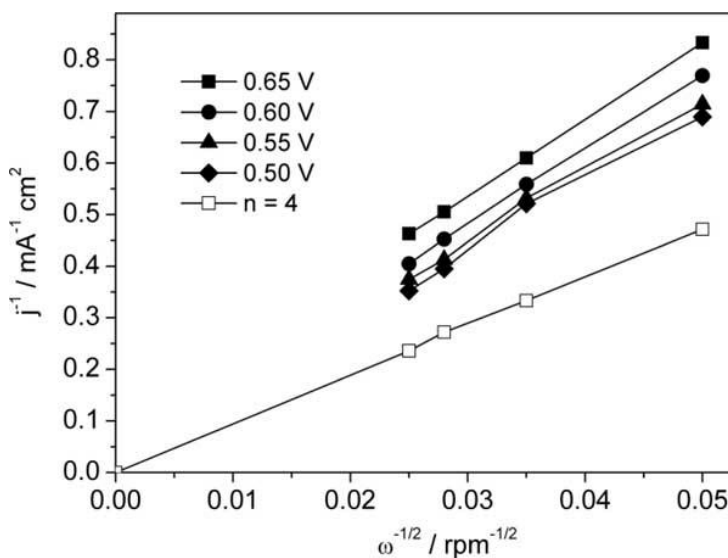


Figure 5. Levich-Koutecky plots corresponding to the experimental data of Pt-Co/MWCNT (from Figure 4).

Taking experimental values from the mixed controlled region corresponding to Pt-Co/MWCNT in Figure 4, $1/j$ vs. $1/\omega^{1/2}$ plots at different potentials are shown in Figure 5. The plots show linearity and parallelism, indicating first-order kinetics with respect to O_2 [23]. The theoretical slope for a $4 e^-$ transfer reaction is also depicted in Figure 5, based on calculations with the relationship:

$$B = 0.2nFD^{2/3}\nu^{-1/6}c_{O_2} \quad (3)$$

where 0.2 applies when ω is expressed in rpm, D is the diffusion coefficient of oxygen in sulfuric acid (1.4×10^{-5} cm²/s), ν is the kinematic viscosity of sulfuric acid (1.0×10^{-2} cm/s), c is the bulk concentration of oxygen (1.1×10^{-6} mol/cm³), F is the Faraday constant (96,500 C) and n is the number of electrons transferred [22, 24]. Clearly, the experimental lines in Figure 5 come near the theoretical 4 e⁻ transfer slope. Calculations indicate that the slopes derived from this Figure correspond to a transfer of nearly 3.6 e⁻, suggesting that the ORR at the home-prepared Pt-Co/MWCNT alloy proceeds via an overall mechanism that leads almost totally to the formation of H₂O.

Notably, the i_r measured at Pt/C and Pt-Co/MWCNT in Figures 3 and 4 is very small, related to the i_d . The percentage of H₂O₂ formed at the Pt-Co/MWCNT catalyst can be calculated with equation (4) [25, 26]. In this equation, N is the collection efficiency, taken here as 0.25. At the same time, the number of the electrons transferred estimated from Levich-Koutecky plot in Figure 5 was confirmed by using equation (5) [27]:

$$\% H_2O_2 = \frac{200i_r/N}{i_d+i_r/N} \quad (4)$$

$$n = \frac{4i_d}{i_d+i_r/N} \quad (5)$$

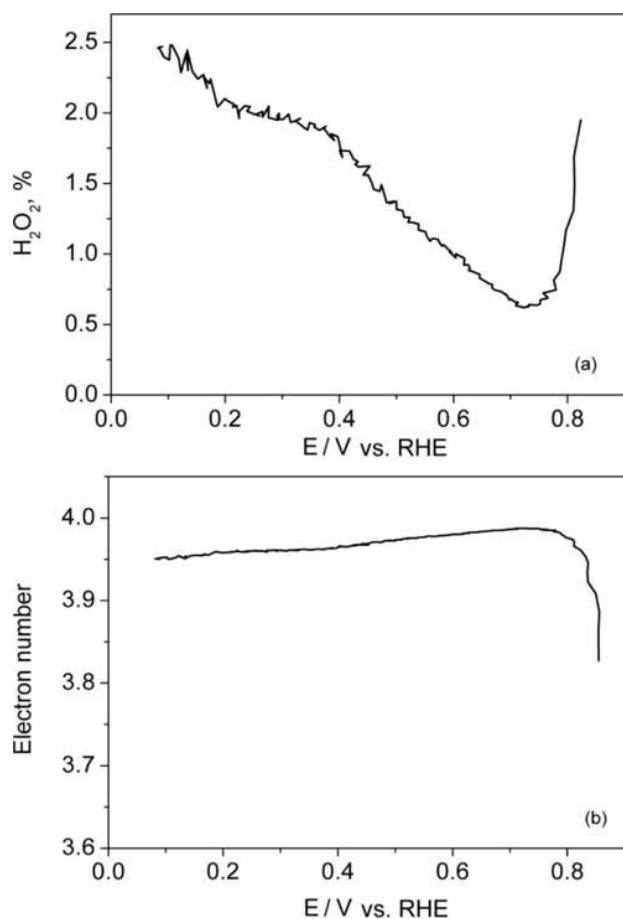


Figure 6. H₂O₂ generated and electron number transferred at Pt-Co/MWCNT during the ORR.

Figure 6 (a) shows the H_2O_2 fraction formed at Pt-Co/MWCNT. The production of H_2O_2 starts increasing at potentials below 0.75 V. However, the results indicate that the alloy produces only 0.6 - 2.5 % H_2O_2 , indicating that O_2 is reduced via a 4 e^- transfer to produce water. In Figure 6(b), the electron number at the Pt-Co/MWCNT electrocatalyst, calculated from equation (5), approaches a value of 4. This number is higher than that determined from the Levich-Koutecky plots (i.e., ~ 3.6 electrons). However, we may conclude that both results correlate well and indicate that the number of electrons transferred at Pt-Co/MWCNT during the ORR is close to 4, confirming a very small production of H_2O_2 and H_2O as the main product.

3.3. Selectivity and tolerance of Pt/C and Pt-Co/MWCNT during the ORR

Figure 7(a) shows the behavior of Pt/C during the ORR in the absence and presence of 0.5M $\text{C}_2\text{H}_6\text{O}_2$ at the rotating speed of 1600 rpm.

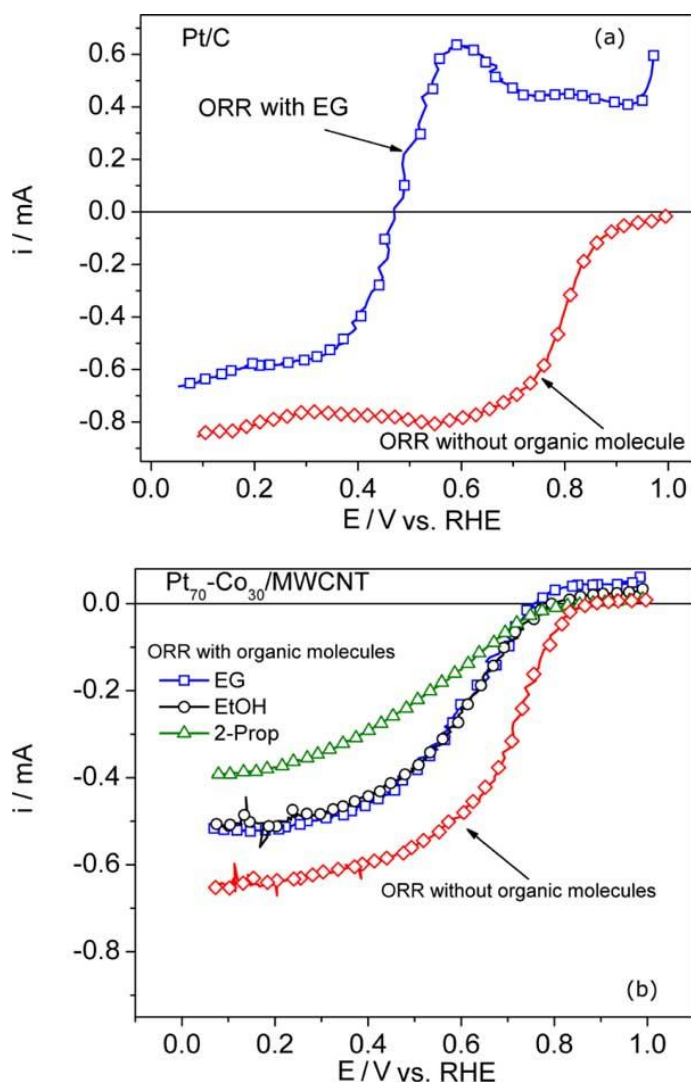


Figure 7. ORR in the absence and presence of liquid fuels. (a) Pt/C; (b) Pt-Co/MWCNT. Scan rate: 10 mV/s. Electrolyte: 0.5 MH_2SO_4 or 0.5M H_2SO_4 + 0.5M (organic fuel). ω : 1600 rpm.

The poor electrochemical selectivity of Pt/C for the ORR under DOFC conditions is clearly demonstrated (i.e., the curve of the ORR with EG). Due to the well-known electrochemical depolarization of Pt-alone cathodes by liquid fuels as shown in references [11, 22 and 28], this material was evaluated only in the presence of EG.

The current (i) – potential (E) behavior of Pt-Co/MWCNT during the ORR in the presence of EtOH, EG or 2-Prop is shown in Figure 7(b). For comparison, the LSV of the ORR without organic molecules is also depicted in this Figure. All polarization curves were taken at 1600 rpm. The selectivity and high degree of tolerance of the alloy to the three organic molecules is clearly demonstrated, indicating a multi-fuel tolerance capability. No current peaks associated to the oxidation of the liquid fuels emerged in the potential range studied here. It can be observed that the $i - E$ characteristics in the electrolyte containing EtOH or EG are quite similar. On the contrary, the i values in the presence of 2-Prop seem to decrease at higher overpotentials (i.e., potentials more negative than 0.6 V). However the selectivity and tolerance characteristics of the alloy are definitively better than those of Pt/C, in good agreement with the literature [3, 11].

3.4. EIS spectra of Pt/C and Pt-Co/MWCNT: ORR without and with organic molecules

EIS data were fitted with the circuit shown in Figure 8 [29-32]. The elements have the following meanings: R_1 is the solution ohmic resistance; R_{ct} is the charge transfer resistance; CPE is a constant phase element, used instead of a capacitance due to the inhomogeneous surface of the electrode [29-31].

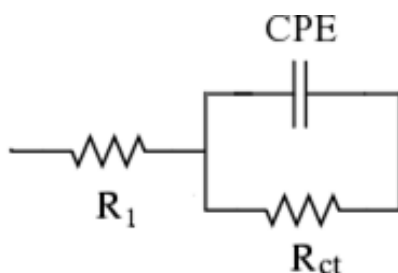


Figure 8. Equivalent circuit used to fit the experimental EIS data.

Figure 9 shows the complex plane plots of Pt/C in O_2 -saturated solution without organic substances. The plots show single time-constant arcs. Increasing the polarization from 854 mV to 754 mV reduces the ORR charge transfer resistance (R_{ct}) because of the enhanced electrochemical kinetics [29], but a further increase to 654 mV results in a larger resistance. The increase in R_{ct} at such potential indicates a transition from an electrochemical kinetic dominated process to a mass transport dominated process with increasing polarization. At higher polarizations in Figure 9(b), the impedance spectra are dominated by the diffusion of species. Thus, the R_{ct} values become progressively larger.

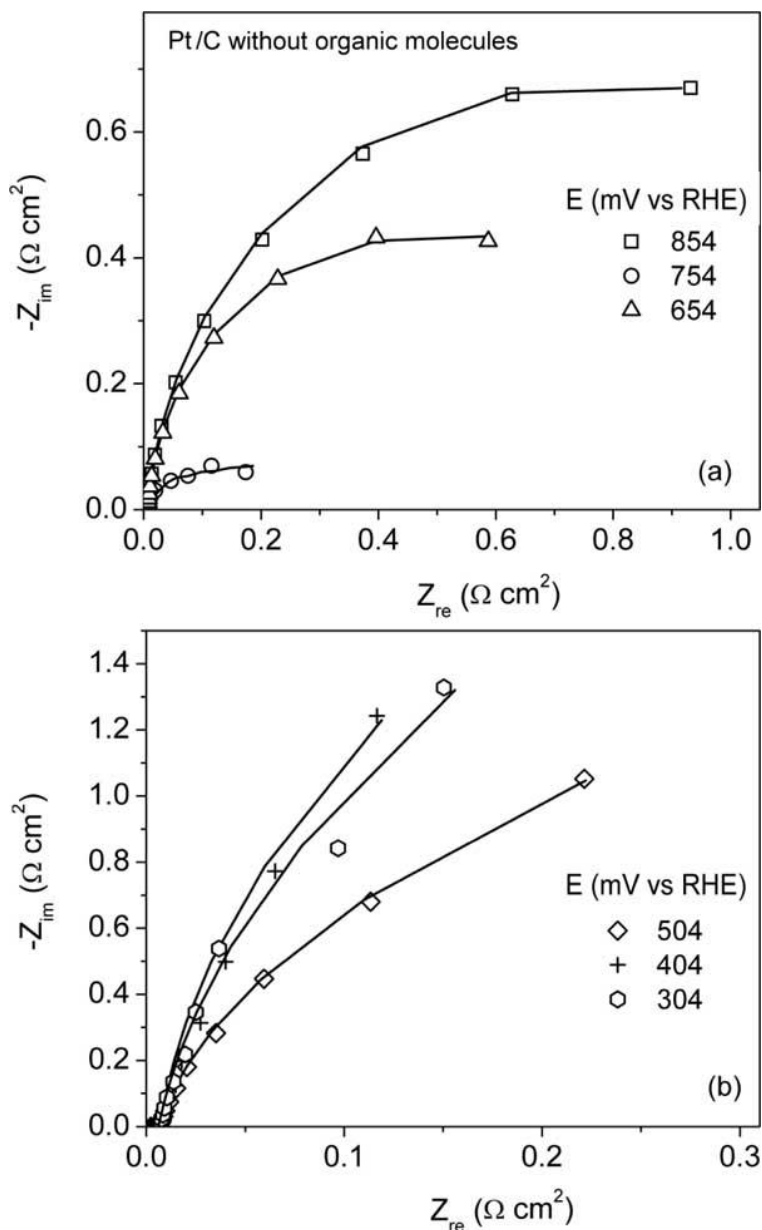


Figure 9. Complex plane plots corresponding to Pt/C in O_2 saturated electrolyte without organic molecules. Symbols: measured data; lines: fitted results.

Figure 10 depicts the impedance spectra of Pt/C in the O_2 -saturated solution containing 0.5M $\text{C}_2\text{H}_6\text{O}_2$. Clearly, the spectra remains one-arc plots over the polarization conditions indicating that the ORR mechanism remains unchanged in the presence of EG.

This behavior is analogous to the results in the presence of methanol reported elsewhere [30-32]. However, it should be noted that the R_{ct} derived from Fig. 10 (a) and (b) exhibits a peak at 654 mV. This potential corresponds to the region of peak maximum due to the oxidation of ethylene glycol in Figure 7, thus, this reaction should be the dominant mechanism. The behavior of Pt/C at 654 mV shows that the charge transfer becomes slower, indicating the presence of adsorbed species, e.g., reaction intermediates arising from the oxidation of EG that might depolarize the Pt surface, such as oxalic acid or glycolic acid [33], or OH_{ads} [34].

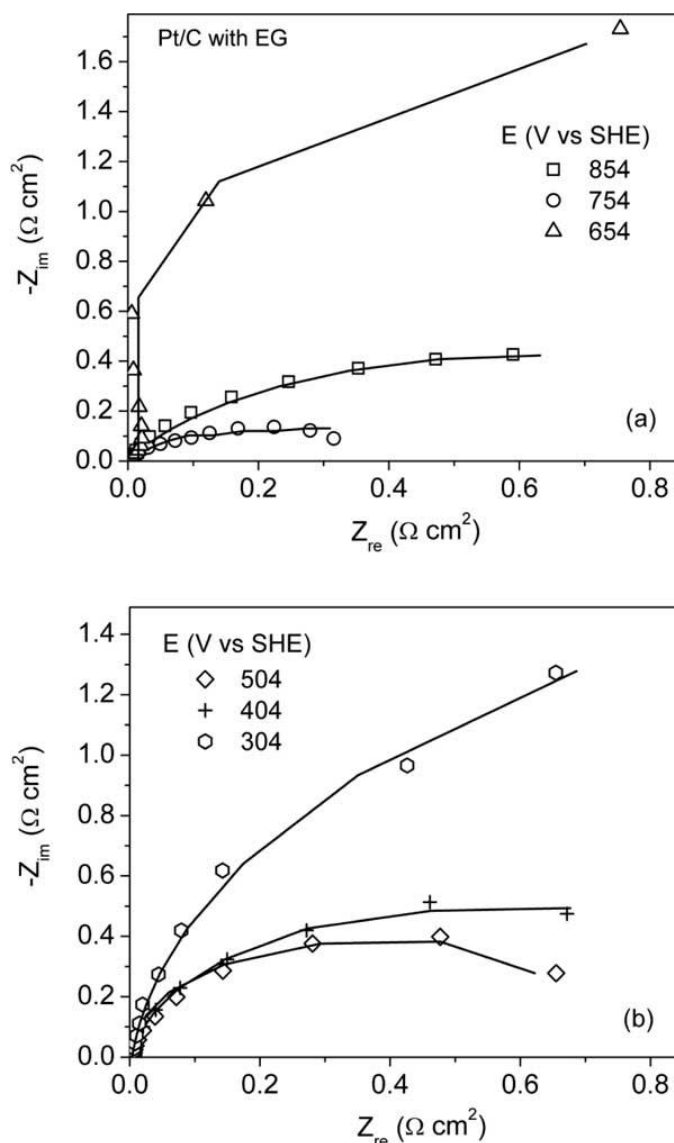


Figure 10. Complex plane plots corresponding to Pt/C in O_2 saturated electrolyte containing 0.5M $\text{C}_2\text{H}_6\text{O}_2$. Symbols: measured data; lines: fitted results.

At higher ORR overpotentials (Figure 10b), the mass transport processes at the electrode are dominant and R_{ct} shows increased values. Interestingly, R_{ct} at 504, 404 and 304 mV in the presence of EG are smaller than the corresponding values without EG (Figure 9b). The trend of R_{ct} with and without EG at the Pt/C electrocatalyst can be clearly observed in the plots depicted in Figure 11.

Contrary to what could be expected from the results in Figure 7(a), where the depolarization of Pt/C is evident in the presence of EG, and therefore an increase in R_{ct} might be the most likely outcome, the competitive reduction/oxidation reactions that are taking place at the surface proceed in such a fashion that the resistance is smaller. Thus, even though the overall electrochemical performance of Pt/C during the ORR in the EG-containing solution decreases in terms of onset potential and ORR current, the charge transfer resistances from Nyquist plots suggest that the Pt catalytic sites may not be completely blocked by the organic fuel or its intermediates at such high polarization potentials.

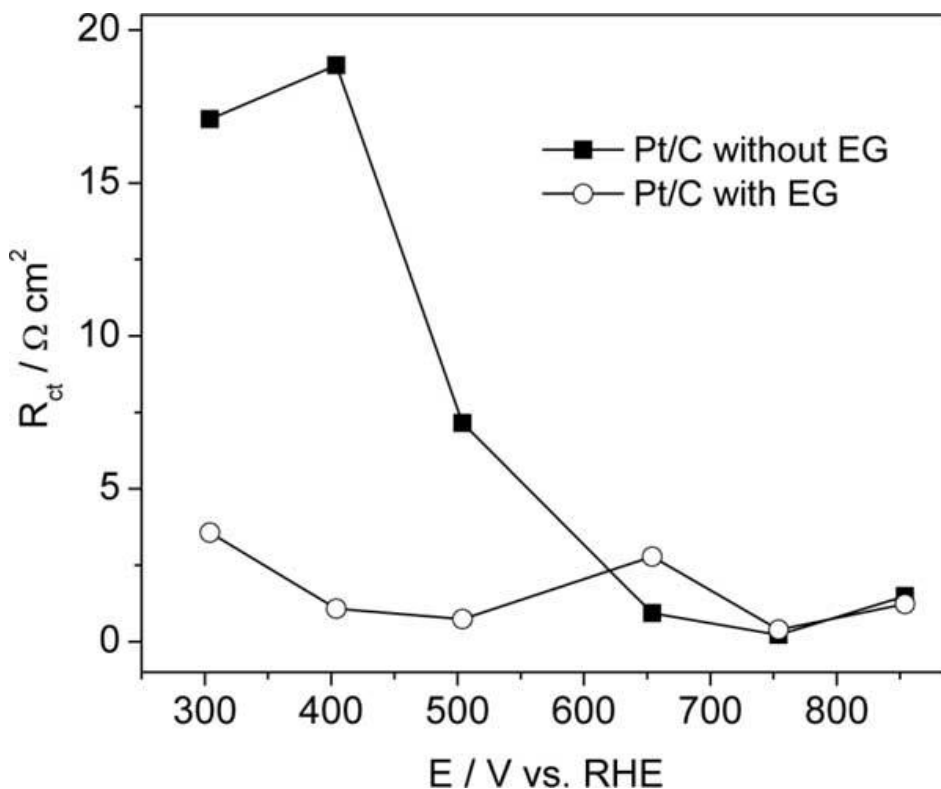


Figure 11. R_{ct} values of the ORR at Pt/C in the absence and presence of 0.5M $C_2H_6O_2$.

Another particular feature of the spectra in Figure 10 is the absence of an inductive behavior. In previous reports, low frequency inductive loops appeared in the presence of methanol at Pt-alone cathodes [30-32, 35]. The authors attributed the presence of such loops to the relaxation of the adsorbed intermediates of the ORR [30], or to the presence of CO at high polarization [31]. Our results indicate that the competitive reaction between O_2 and EG taking place at Pt/C proceeds in a different way compared to the competitive reaction between O_2 and MeOH. As a result, the intermediates formed from the EG oxidation reaction (which besides CO or OH-like species are totally different from those produced from the MeOH oxidation reaction [33]) are not as strongly adsorbed as to produce the appearance of a well-defined inductive loop.

In a recent work by Zelenay *et al.* regarding the cathode behavior of Pt/C in the presence of methanol [31], the authors divided the developing reactions in ORR-part and fuel oxidation-part. Considering this combined scheme, an explanation to the smaller R_{ct} in the EG-containing electrolyte (Figure 10b) at high polarization potentials can be as follows:

i) At the high ORR polarization studied in this work, $C_2H_6O_2$ can be oxidized at Pt catalysts [36]. Making a correlation between the LSV with EG in Figure 7(a) and the Nyquist plots in Figure 10(b), the smaller R_{ct} values at high polarization may be associated to a faster EG oxidation-part, i.e., the high catalytic activity of Pt/C for the EG oxidation reaction clearly has a positive effect in decreasing the charge transfer resistances at 504, 404 and 304 mV.

ii) The oxidation of EG may form OH-like species [33, 36], i.e., similar to the oxidation of EtOH and MeOH [37]. Such intermediates take part in the oxidation of CO_{ads} to CO_2 [37] and also in

the reduction of adsorbed O species on Pt catalytic sites to form H₂O [38-40]. This reduction reaction might be dominant at higher overpotentials, particularly at 304 mV, where the current in Figure 7(a) is clearly more related to the ORR-part. It should be mentioned that a recent report shows that at high surface coverage of OH-like species, the ORR may be hindered at Pt-based catalysts [41]. However, the presence of such species and their involvement in one of the steps to produce water during the ORR is widely accepted and has been proposed from experimental and theoretical studies by different groups [38-40]. The degree of surface coverage and the influence of this parameter on the phenomena discussed here-above in the presence of the organic molecule is out of the scope of this study.

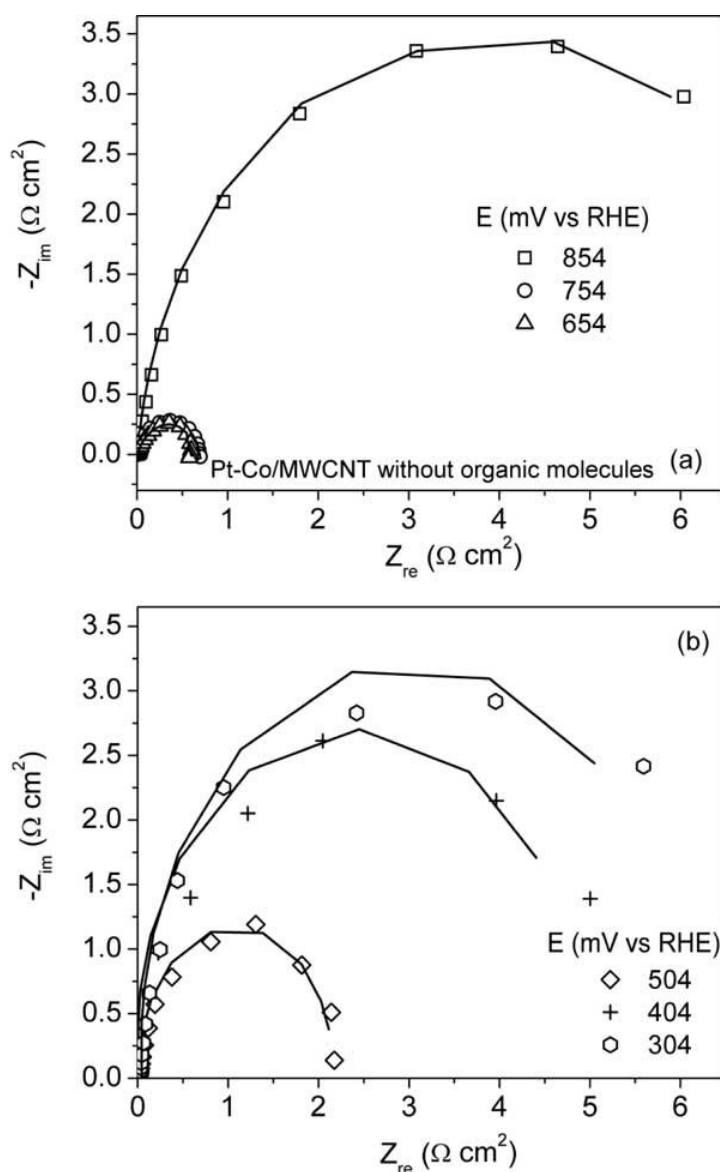


Figure 12. Complex plane plots at Pt-Co/MWCNT in O₂ saturated electrolyte without organic molecules. Symbols: measured data; lines: fitted results.

Figure 12 shows the Nyquist plots of the ORR at the Pt-Co/MWCNT alloy without fuels. Similar to Pt/C, the shape of the spectra at low and high polarizations indicate one mechanism with a

single time constant taking place at the electrocatalyst. It can be observed that R_{ct} becomes smaller in the 854 to 654 mV interval, but at 504 mV the mass transport processes become more important compared to the transport at 754 and 654 mV. Therefore R_{ct} becomes higher at increasing polarization (Figure 12b). Thus, at different degrees of polarization the impedances related to the ORR-part are controlled by electrochemical kinetics or mass transport limitations, in good agreement with the literature [29].

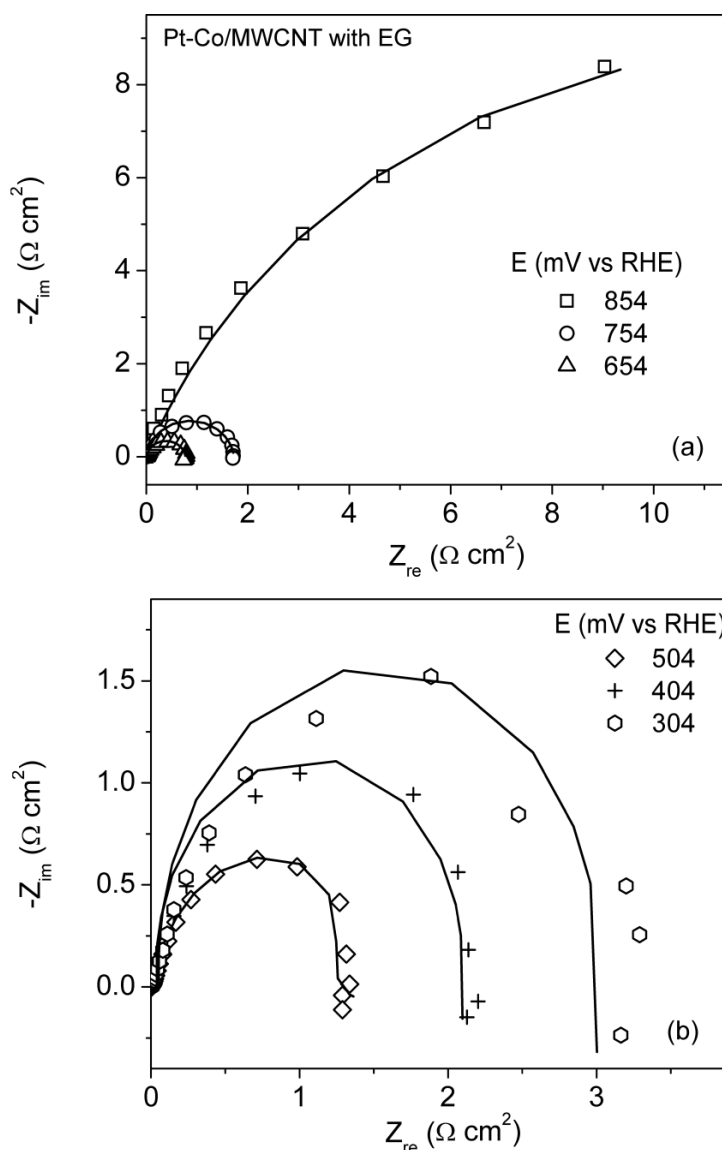


Figure 13. Complex plane plots at Pt-Co/MWCNT in O_2 saturated electrolyte containing 0.5M $\text{C}_2\text{H}_6\text{O}_2$. Symbols: measured data; lines: fitted results.

Figure 13 depicts the complex plane spectra of the ORR at Pt-Co/MWCNT in the presence of 0.5M EG. As in the case of Pt, the response of the alloy for the ORR remains a one-arc mechanism. At low ORR overpotentials (854 and 754 mV) the values of R_{ct} increase (Figure 13a), related to the values in the absence of organic fuel (Figure 12a). This behavior of Pt-Co at low polarization is different from

that of Pt/C in the absence and presence of EG (Figures 9a and 10a, respectively) in which R_{ct} decreased at 854 mV but increased at 754 mV once the fuel was added to the electrolyte. This difference is evidently related to the specific reactions taking place at each electrocatalyst, because at low polarization potentials the dominant reaction on Pt/C clearly is the EG oxidation-part (see Figure 7a), with an apparently hindered ORR-part being developed at such cathode. Meanwhile, at Pt-Co/MWCNT the process taking place is a competitive reaction with a more important ORR-part along with the EG oxidation-part (see figure 7b). Therefore, even though in terms of onset potential the behavior of Pt-Co in the solution containing EG is significantly better than that of Pt, at these polarization potentials there is a mixed reaction at the surface of the alloy that results in larger charge transfer resistances at 854 and 754 mV.

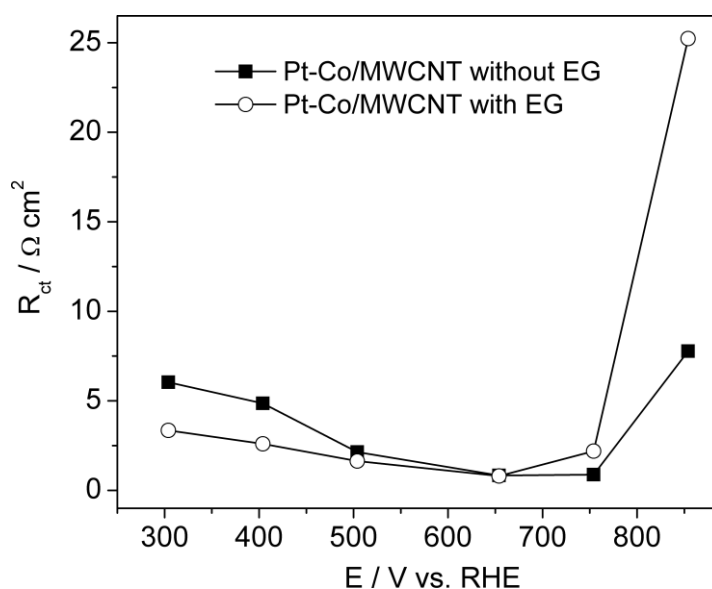


Figure 14. R_{ct} values of the ORR at Pt-Co/MWCNT in the absence and presence of 0.5M $C_2H_6O_2$.

Meanwhile, at high polarization potentials the values of R_{ct} at the alloy with EG (Figure 13b) are smaller compared to the values without EG (Figure 12b), similar to the behavior of Pt/C at such potentials. Such trend of R_{ct} values at Pt-Co/MWCNT can be observed in Figure 14.

An apparent semi-inductive behavior seems to show at the Pt-Co alloy in Figure 13(b). However, only a few dispersed points can be observed in the fourth quadrant. Therefore, it cannot be concluded that a clear inductive loop related to the presence of EG or reaction intermediates is a characteristic of the spectra in Figure 13(b). Such feature makes the competitive process involving the ORR and the EG oxidation reaction different from the case when methanol was the liquid fuel [30, 31].

Thus, an explanation can be given in the same fashion as that for Pt here-above. But additionally and given the selectivity and tolerance of Pt-Co/MWCNT to EG shown in Figure 7(b), the following interpretation can be considered as well:

i) A weak adsorption of EG at Pt-Co can be seen in Figure 7(b), allowing for free Pt catalytic sites in the alloy to catalyze the ORR-part.

ii) Weakly adsorbed EG molecules can be oxidized at the catalytic surface of the alloy at the potentials studied here.

iii) The reactions related to the oxidation of adsorbed EG generate OH-like species [33, 36] that contribute to a faster reaction of adsorbed O species to form H₂O [38-40]. Thus, the lower R_{ct} values at high polarization correspond to a faster and dominant ORR-part in a process that involves both the cathodic and anodic reactions. This interpretation is in good agreement with the results published previously by Zelenay *et al.* [31].

Nyquist plots of the ORR at Pt-Co/MWCNT in the presence of EtOH and 2-Prop were also obtained in this study (not shown). Overall, the shape and characteristics of the spectra are similar to those with EG in Figure 13 indicating that the ORR mechanism with all three fuels might be analogous. The corresponding R_{ct} values in the presence of EtOH and 2-Prop are given in Table 2. Our results in acid medium indicate that the alternative fuels studied here are good candidates to replace MeOH in fuel cells. Previous reports indicate that the electro-oxidation activity of EtOH and 1-Propanol was better in alkaline medium compared to MeOH [42].

Table 2. R_{ct} values of the ORR at Pt-Co/MWCNT in the presence of C₂H₅OH and C₃H₈O.

R _{ct} @ Pt-Co/MWCNT (Ω cm ²)		
E (mV)	O ₂ with 0.5M C ₂ H ₅ OH	O ₂ with 0.5M C ₃ H ₈ O
854	29.54	38.41
754	3.28	5.25
654	1.18	1.70
504	1.56	1.78
404	2.67	2.18
304	4.06	2.57

Considering the ORR behavior of Pt-Co/MWCNT with EG, EtOH and 2-Prop, it is clear that there is a potential-dependent effect of the oxidation of the three different organic substances. The higher R_{ct} values at low polarization potentials (854, 754 and 654 mV) are due to the adsorption of the organic molecules or their intermediates on the Pt-Co/MWCNT surface, affecting the kinetics of the ORR [30, 32].

At increased polarization potentials (504, 404 and 304 mV) the capacitive arcs become smaller, indicating a faster reaction that involves the ORR-part and the fuels oxidation-part. These results correlate well with the findings by Zelenay *et al.* [31], where the authors found out that at increasing

current densities in their experimental fixture, the diameter of the capacitive circle in the spectrum of a DMFC cathode decreased, due to an acceleration of the electrode processes.

4. CONCLUSIONS

The RRDE results indicate that the ORR at Pt-Co/MWCNT follows a nearly 4 e⁻ mechanism. Moreover, LSVs of the ORR in the presence of C₂H₅OH, C₂H₆O₂ or C₃H₈O confirm the high selectivity and tolerance of this cathode.

The EIS results of the ORR at Pt-Co/MWCNT and Pt/C in the absence and presence of the liquid fuels show one-arc spectra, indicating that the ORR mechanism at the cathodes may not change when those substances were in the solution. The behavior of Pt-Co/MWCNT for the ORR with EG, EtOH or 2-Prop is similar. Thus, the ORR mechanism with the three organic molecules is proposed to be analogous. At high polarization potentials, the R_{ct} values at Pt-Co/MWCNT and Pt/C in the presence of the fuels are smaller than the values in their absence. This is particularly interesting in the case of Pt/C because an increase in R_{ct} might be expected due to the fact that the electrochemical behavior of this cathode during the ORR is appreciably poor in the solution containing EG. The results indicate that both the ORR-part and the fuel oxidation-part are kinetically enhanced at the high polarization potentials studied in this work. It is proposed that the fuels oxidation reaction forms OH-like species that participate in the steps to reduce O_{ads} species to water. The degree of surface coverage by these intermediates and their effect on the impedance measurements in the presence of organic molecules is out of the scope of this study.

Noteworthy is the fact that no inductive loops were observed at Pt-Co/MWCNT or Pt/C. These results differ from reports in the literature where an inductive behavior clearly appeared when MeOH was added to the solution. Thus, the oxidation of the three fuels studied here may proceed by a mechanism distinct to MeOH where the intermediates produced are not as strongly adsorbed at the catalytic sites of the cathodes as the intermediates formed during the methanol oxidation reaction.

ACKNOWLEDGEMENTS

The authors wish to thank the National Council for Science and Technology (Conacyt-México) for financial support through Grant No. 79870.

References

1. E. Antolini, J.R.C. Salgado, L.G.R.A. Santos, G. Garcia, E.A. Ticianelli, E. Pastor, E.R. Gonzalez. *J. Appl. Electrochem.*, 36 (2006) 355.
2. F.J. Rodríguez Varela, O. Savadogo. *J. Electrochem. Soc.*, 155 (2008) B618.
3. F.J. Rodríguez Varela, O. Savadogo. *Asia-Pac. J. Chem. Eng.*, 4 (2009) 17.
4. J. Arun Kumar, P. Kalyani, R. Saravanan. *Int. J. Electrochem. Sci.*, 3 (2008) 961.
5. M. Umeda, H. Sugii, I. Uchida. *J. Power Sources*, 179 (2008) 489.
6. V. Baglio, A. Di Blasi, C. D'Urso, V. Antonucci, A.S. Aricò, R. Ornelas, D. Morales-Acosta, J. Ledesma-Garcia, L.A. Godinez, L.G. Arriaga, L. Alvarez-Contreras. *J. Electrochem. Soc.*, 155 (2008) B829.

7. Y. Qian, W. Wen, P.A. Adcock, Z. Jiang, N. Hakim, M.S. Saha, S. Mukerjee. *J. Phys. Chem. C*, 112 (2008) 1146.
8. H. Yang, C. Coutanceau, J.M Léger, N. Alonso-Vante, C. Lamy. *J. Electroanal. Chem.*, 576 (2005) 305.
9. S. Mukerjee, S. Srinivasan. *J. Electroanal. Chem.*, 357 (1993) 201.
10. Q. Huang, H. Yang, Y. Tang, T. Lu, D.L. Akins. *Electrochem. Commun.*, 8 (2006) 1220.
11. D. Morales-Acosta, L.G. Arriaga, L. Alvarez-Contreras, S. Fraire Luna, F.J. Rodríguez Varela. *Electrochem. Commun.*, 11 (2009) 1414.
12. W.J. Zhou, W.Z. Li, S.Q. Song, Z.H. Zhou, L.H. Jiang, G.Q. Sun, Q. Xin, K. Poulianitis, S. Kontou, P. Tsiakaras. *J. Power Sources*, 131 (2004) 217.
13. F.J. Rodríguez Varela, S.E. González Ramírez, R. Dabek Klapco. *J. New Mat. Electrochem. Systems*, 12 (2009) 9.
14. V. Livshits, A. Philosoph, E. Peled. *J. Power Sources*, 178 (2008) 687.
15. V. Livshits, E. Peled. *J. Power Sources*, 161 (2006) 1187.
16. V. Selvaraj, M. Vinoba, M. Alagar. *J. Colloid Interface Sci.*, 322 (2008) 537.
17. S.S. Gupta, J. Datta. *J. Chem. Sci.*, 117 (2005) 337.
18. U.B. Demirci. *Environ. Int.*, 35 (2009) 626.
19. E. Peled, V. Livshits, T. Duvdevani. *J. Power Sources*, 106 (2002) 245.
20. S.K. Natarajan, J. Hamelin. *J. Electrochem. Soc.*, 156 (2009) B210.
21. O. Savadogo, F. J. Rodríguez Varela. *ECS Trans.*, 1 (2006) 331.
22. F.J. Rodríguez Varela, S. Fraire Luna, O. Savadogo. *Energies*, 2 (2009) 944.
23. G. Ramos-Sanchez, H. Yee-Madeira, O. Solorza-Feria. *Int. J. Hydrogen Energy*, 33 (2008) 3596.
24. B.R. Camacho, M.T. Rodriguez, O. Solorza-Feria. *J. New Mat. Electrochem. Systems*, 12 (2009) 43.
25. L. Liu, H. Kim, J.-W. Lee, B.N. Popov. *J. Electrochem. Soc.*, 154 (2007) A123.
26. R. Benítez, A.M. Chaparro, L. Daza. *J. Power Sources*, 151 (2005) 2.
27. C.W.B. Bezerra, L. Zhang, K. Lee, H. Liu, J. Zhang, Z. Shi, A.L.B. Marques, E.P. Marques, S. Wu, J. Zhang. *Electrochim. Acta*, 53 (2008) 7703.
28. P. Nekooi, M. Akbari, M.K. Amini. *Int. J. Hydrogen Energy*, 35 (2010) 6392.
29. Z. Xie, S. Holdcroft. *J. Electroanal. Chem.*, 568 (2004) 247.
30. C.Y. Du, T.S. Zhao, W.W. Yang. *Electrochim. Acta*, 52 (2007) 5266.
31. P. Pielá, R. Fields, P. Zelenay. *J. Electrochem. Soc.*, 153 (2006) A1902.
32. C.Y. Du, T.S. Zhao, C. Xu. *J. Power Sources*, 167 (2007) 265.
33. N. Travitsky, L. Burstein, Y. Rosenberg, E. Peled. *J. Power Sources*, 194 (2009) 161.
34. X. Wang, J.-M. Hu, I.-M. Hsing. *J. Electroanal. Chem.*, 562 (2004) 73.
35. F. Xiao-juan, S. Yan-long, H. Zhong-ai. *Int. J. Electrochem. Sci.*, 5 (2010) 489.
36. A.Serov, C. Kwak. *Appl. Catal. B-Environ.*, 97 (2010) 1.
37. F. Maillard, S. Pronkin, E.R. Savinova, *Handbook of Fuel Cells*, Wolf Vielstich, Hubert A. Gasteiger, Harumi Yokokawa (Eds.), Volume 5, Ch. 7, Wiley, (2009).
38. K. Kinoshita, *Electrochemical Oxygen Technology*, John Wiley & Sons, Inc., N.Y., Chapter 2, (1992).
39. F. Fouda-Onana, O. Savadogo. *Electrochim. Acta*, 54 (2009) 1769.
40. S. Gottesfeld, *Fuel cell catalysis, A surface science approach*, Marc T.M. Koper (Ed.), John Wiley and Sons Inc., Chapter 1, (2009).
41. V.R. Stamenkovic, B. Fowler, B. Simon Mun, G. Wang, P.N. Ross, C.A. Lucas, N.M. Marković. *Science*, 315 (2007) 493.
42. D. Wang, J. Liu, Z. Wu, J. Zhang, Y. Su, Z. Liu, Ch. Xu. *Int. J. Electrochem. Sci.*, 4 (2009) 1672.